L-vacancy decay in heavy elements ($72 \leq Z \leq 82$) by the synchrotron photoionization method

U. Werner
Fakultät für Physik, Universität Bielefeld, D-4800 Bielefeld 1, Federal Republic of Germany

W. Jitschin
Physikalisch-Technische Bundesanstalt, Institut Berlin, D-1000 Berlin 10, Federal Republic of Germany
(Received 26 February 1988)

Employing the novel synchrotron photoionization method, the Coster-Kronig decay yields f_{12}, f_{13}, and f_{23} as well as the ratios of radiative yields ω_1/ω_3 and ω_2/ω_3 have been measured for a series of neighboring heavy elements with a typical uncertainty of ± 0.01 and ± 0.03, respectively. The data for f_{23} and ω_2/ω_3 are compared to published experimental data obtained with the $K\alpha$-$L\alpha$ coincidence method that have small uncertainty; reasonable agreement is found. In contrast, our f_{12} values are considerably smaller (factor of 2–3) than published experimental values obtained by various techniques; this result indicates systematic problems of these techniques. Using the well-known fluorescence yield ω_3 and calculated absolute transition rates of the radiative decay, we have derived absolute transition rates of the nonradiative decay from our experimental data. Comparison of the observed values with theoretical transition rates shows that the theory substantially overestimates the rates of such nonradiative transition channels in which the excess energy carried away by the emitted electron is substantially smaller than the energy of the initial vacancy state.

I. INTRODUCTION

A vacancy in an inner electron shell of an atom is rapidly filled up by an electron from a higher (sub)shell, whereby in a radiative decay a photon and in a nonradiative decay an electron is emitted. In numerous fields ranging from fundamental research on atomic collision processes to quantitative surface analysis by spectroscopic techniques, reliable accurate values of the decay probabilities are required in order to derive the vacancy creation from the observed photons or electrons.[1–4] Beside these important applications, the decay rates provide a stringent test of atomic physics theory, since they reflect the intrinsic evolution of an atom in a nonstationary state. The sum of all decay rates determines the energy width of atomic levels according to Heisenberg's uncertainty principle.

Comprehensive calculations of decay rates exist for the radiative decay, which is basically a one-electron process,[5] as well as for the nonradiative Auger and Coster-Kronig decay, which is basically a two-electron process.[6] Whereas the fluorescent and Auger channels have an excess energy on the order of the initial-state energy, the Coster-Kronig channel has considerably less excess energy[7] (Fig. 1). Some Coster-Kronig transitions are of high importance since they have large transition rates. In case of the L_1 subshell, the Coster-Kronig channel accounts for more than about half of all decays for elements with $Z \geq 12$. Since calculated Coster-Kronig rates are sensitive to various effects,[8] theoretical L_1 yields[9] bear particularly large uncertainties.

Experimentally, a number of methods has been applied to measure decay yields.[10,11] In case of the K shell, the fluorescent (radiative) and Auger (nonradiative) decay probabilities are now known quite well.[12–14] In the case of the L shell, the number of decay parameters is larger; their determination requires the creation of a known number of primary vacancies in the individual L subshells. With the currently available semiconductor detectors, the $K\alpha$-$L\alpha$ coincidence method is a powerful method to determine all yields for the L_3 and L_2 subshells, i.e., ω_3, ω_2, and f_{23}, and uncertainties as small as one or a few percent have been reported recently.[15–17] In this method, the $K\alpha_1$ and $K\alpha_2$ photons are used to identify a primary vacancy in the L_3 and L_2 subshells, respectively. The method fails for the L_1 subshell due to the very small K-L_1 radiative decay rate. Yields of the L_1 subshell have been obtained by applying various coincident as well as noncoincident methods giving results with modest accuracy. The region around $Z \simeq 74,75$ is of particular interest because of the expected onset of the strong L_1-$L_3M_{4,5}$ Coster-Kronig decay channel (Fig. 1). Most work on decay yields so far has been performed by using radioactive isotopes.[10,11] These are not readily available for each element. The proper experimental method and the number of primary vacancies depend on the particular nuclear disintegration process. Accordingly, no comprehensive data sets have been obtained.

Recently a novel and universal method for measuring yields of *all* subshells was introduced which is based on tunable synchrotron radiation.[18,19] As described in detail in Sec. II, it relies on the switching on of the vacancy creation in a particular subshell when the radiation energy is tuned above the subshell ionization threshold. In an exploratory measurement this method has provided stimulating results for Au ($Z=79$). Therefore comprehensive measurements of the photoabsorption and photoemission for a range of elements, $72 \leq Z \leq 82$, have been performed and are presented in the present paper. These have revealed minor effects in the photoionization

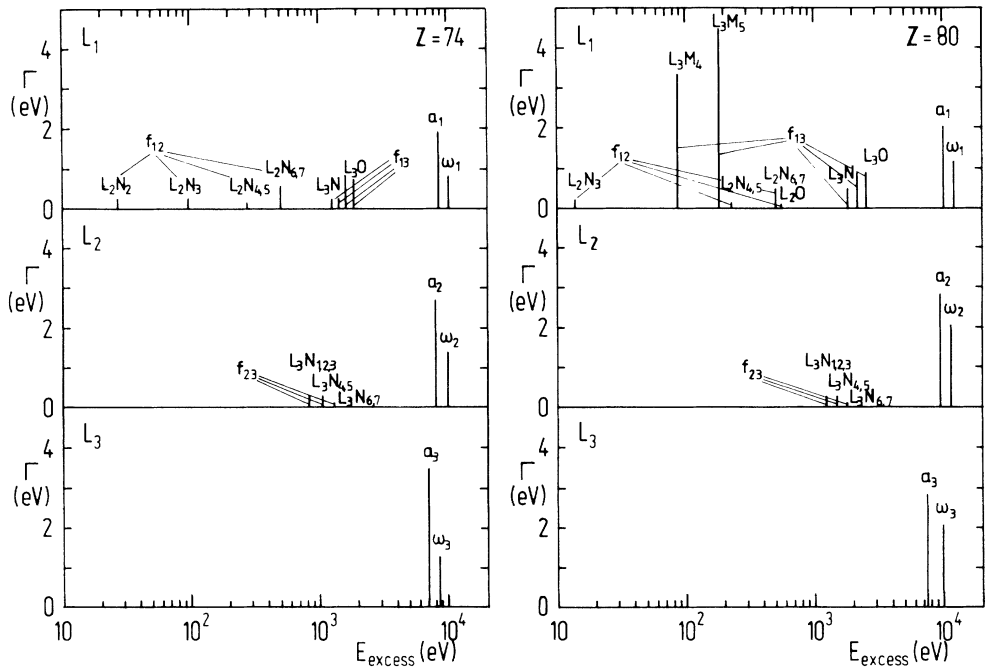

FIG. 1. Calculated absolute decay rates for the L subshells vs excess energy of the emitted particle for $_{74}$W (left) and $_{80}$Hg (right) (Refs. 5 and 6). The most striking difference between these two elements is the strong L_1-$L_3M_{4,5}$ Coster-Kronig channel which is energetically allowed only for $_{80}$Hg.

process[20] which are not negligible in the extraction of decay yields from the photoemission data. In Sec. III some experimental details are described. In Sec. IV the photon-energy dependence of L-subshell photoionization cross sections is discussed. In Sec. V the obtained data are presented and compared to other experimental work; some of the data have already been presented in Ref. 21. Finally, in Sec. VI additional information from theoretical calculations is employed in order to convert the experimental data to absolute decay rates; these are directly compared to theoretical predictions of nonradiative rates.

II. SYNCHROTRON PHOTOIONIZATION METHOD

The applied novel method relies on the creation of primary vacancies by photoionization with tunable photon energy and the detection of the induced fluorescence (or Auger electrons) (Fig. 2). Photoionization offers essential advantages as compared to other processes of vacancy creation. First, the ionization of a particular subshell can be switched on and off by tuning the energy of the primary photons across the ionization threshold. Second, the cross section of an individual subshell is known with comparatively high accuracy, since theoretically photoionization can be well predicted and experimentally it can be directly obtained from x-ray attenuation studies. Third, photoionization really produces the desired single-vacancy state; it suffers less by outer-shell ionization than ionization by charged-particle impact; it also does not leave a $Z+1$ outer-electron configuration of a Z nucleus as does the electron-capture decay in nuclear disintegration.

The fluorescence (or the Auger electrons) emitted in the vacancy decay is detected at various energies of the primary photons. Spectroscopic techniques are applied in the detection in order to identify the subshell from which the emitted decay product originated. The intensity of the fluorescence (or the Auger electrons) is a measure for the number of vacancies created directly by photoionization or indirectly by Coster-Kronig cascades. This is illustrated for L-subshell photoionization and fluorescence detection in Fig. 2; the equations for this case are now given.

The intensity I_{L_3} of a line originating from the L_3 subshell (e.g., $L\alpha$) is proportional to the total L_3 vacancy production,

$$I_{L_3} \propto \begin{cases} \sigma_{L_3} & \text{for } E_{L_3} < E_\gamma < E_{L_2} \\ \sigma_{L_3} + f_{23}\sigma_{L_2} & \text{for } E_{L_2} < E_\gamma < E_{L_1} \\ \sigma_{L_3} + f_{23}\sigma_{L_2} + (f_{13} + f_{12}f_{23})\sigma_{L_1} & \text{for } E_{L_1} < E_\gamma < E_K . \end{cases} \tag{1}$$

σ_{L_3}, σ_{L_2}, and σ_{L_1} denote the ionization cross sections of the L subshells; E_{L_3}, E_{L_2}, and E_{L_1} are the ionization thresholds; E_γ is the primary photon energy.

In the sum, the first term corresponds to direct L_3 ionization, whereas the other two terms describe a Coster-Kronig vacancy transfer from the L_2 and L_1 subshells, respectively. Here we tacitly assume that the emission probability of the line is not affected by the spectator va-

cancy produced by a Coster-Kronig transition. With the measured line intensity versus E_γ and the known ionization cross sections one obtains the Coster-Kronig yields f_{23} and $f_{13}+f_{12}f_{23}$.

The intensity I_{L_2} of a line originating from the L_2 subshell (e.g., $L\gamma_1$) is proportional to the total L_2 vacancy production,

$$I_{L_2} \propto \begin{cases} \sigma_{L_2} & \text{for } E_{L_2} < E_\gamma < E_{L_1} \\ \sigma_{L_2} + f_{12}\sigma_{L_1} & \text{for } E_{L_1} < E_\gamma < E_K . \end{cases} \quad (2)$$

Similar to the preceding case, one obtains f_{12}. Since f_{12} and f_{23} are now known, the measured $f_{13}+f_{12}f_{23}$ can be portioned into its components to get f_{13}. The portioning does not introduce much additional uncertainty since for all elements $f_{12}f_{23} \ll f_{13}$ and thus the $f_{12}f_{23}$ term is only a minor contribution.

The total intensity I of the fluorescence radiation is

$$I \propto \begin{cases} \omega_3\sigma_{L_3} & \text{for } E_{L_3} < E_\gamma < E_{L_2} \\ \omega_3(\sigma_{L_3}+f_{23}\sigma_{L_2})+\omega_2\sigma_{L_2} & \text{for } E_{L_2} < E_\gamma < E_{L_1} \\ \omega_3[\sigma_{L_3}+f_{23}\sigma_{L_2}+(f_{13}+f_{12}f_{23})\sigma_{L_1}] & \\ \quad +\omega_2(\sigma_{L_2}+f_{12}\sigma_{L_1})+\omega_1\sigma_{L_1} & \text{for } E_{L_1} < E_\gamma < E_K . \end{cases} \quad (3)$$

The proportionality constant depends on instrumental parameters, e.g., primary photon flux, detector solid angle, and efficiency which can be determined. Thus in principle it is possible to obtain the fluorescence yields ω_i. However, we did not make use of this possibility, since the uncertainty of the constant and thus of the fluorescence yields would be rather large. In contrast, the ratios ω_i/ω_j are independent of the constant and can be extracted from the set of equations (3). Therefore it is advantageous to adopt the accurate ω_3 values from the literature to determine the less accurately known ω_2 and ω_1 from the measured ratios ω_2/ω_3 and ω_1/ω_3.

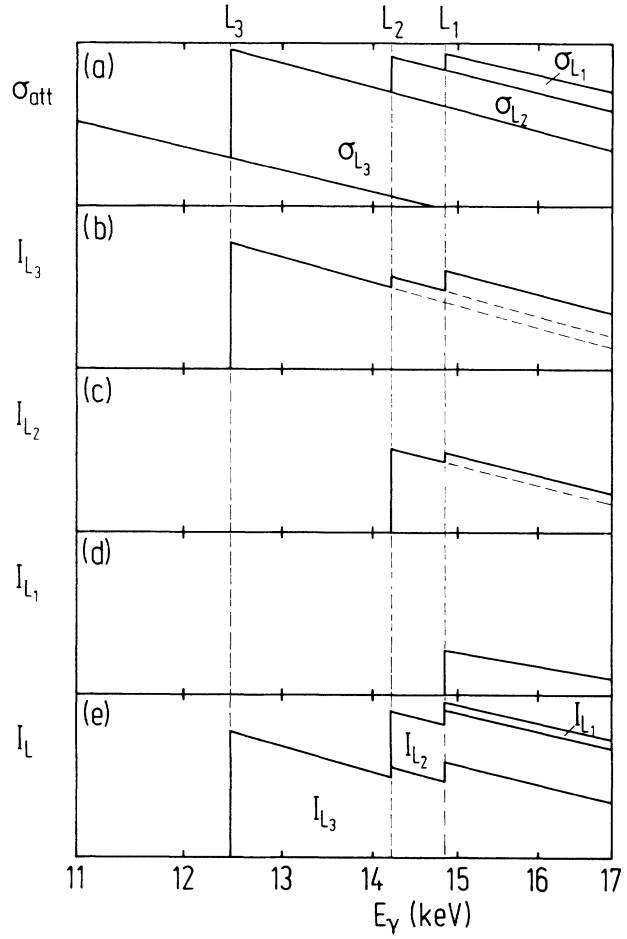

FIG. 2. Principle of the applied method. (a) Photoattenuation cross section (logarithmic scale) and its partition into the contributions from the individual subshells. (b) Intensity of an x ray or Auger line originating from the L_3 subshell. (c) Same as (b), but from the L_2 subshell. (d) Same as (b), but from the L_1 subshell. (e) Total L-fluorescence or L-Auger intensity, i.e., summed over all L subshells, the individual contributions are indicated. Figures (a)–(e) are approximately to scale for $_{80}$Hg.

III. EXPERIMENT

The measurements were performed on the Röntgen-Monochromator (ROEMO) instrument at the Hamburg Synchrotron Radiation Laboratory (HASYLAB) (Fig. 3). Data were taken at several beam times with different operating conditions of the storage ring Doppel-Ring-Speicher II (DORIS II). Typical operating values are an electron energy of 5 GeV and a ring current of 25–40 mA. The radiation was monochromatized by a Si(111) nondispersive double-crystal monochromator; harmonics were suppressed by giving the second crystal a slight offset as compared to the first one.[22] The x-ray energy scale of the monochromator was calibrated by recording absorption edges whose energies are well known.[23] The energy bandwidth of the radiation is determined by its angular collimation and amounted to a few eV.

For most of the investigated elements two sample foils of this element were used: A "thick" one (4–10 μm, self-supporting) with reasonable attenuation for the absorption measurements and a "thin" one (0.025–0.25 μm, supported) (Table I) with only minor attenuation for the fluorescence measurements. The thick foil was mounted

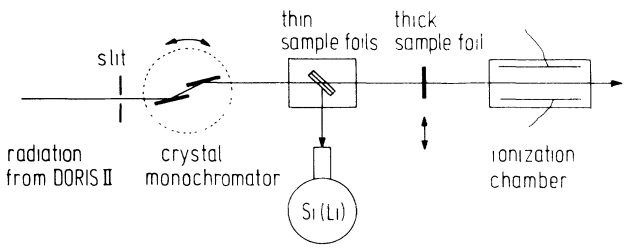

FIG. 3. Experimental setup.

TABLE I. Compilation of the sample-foil–normalization-foil combinations used in the fluorescence measurements. All foils were evaporated on a Mylar support of 3-μm thickness except the Au-Cu combination.

Sample foil	Thickness (μm)	Normalization foil	Thickness (μm)
$_{72}$Hf	0.025	$_{25}$Mn	0.025
$_{73}$Ta	0.025	$_{25}$Mn	0.025
$_{74}$W	0.025	$_{25}$Mn	0.025
$_{77}$Ir	0.025	$_{25}$Mn	0.025
$_{78}$Pt	0.025	$_{25}$Mn	0.025
$_{79}$Au	0.2	$_{29}$Cu	0.25
$_{82}$Pb	0.025	$_{29}$Cu	0.025

behind the thin one (Fig. 3); thus it was possible to make the attenuation measurements by simply moving the thick foil in and out of the beam and monitoring the transmitted intensity by the ionization chamber while the time-consuming detection of the fluorescence [limited by the count-rate capability of the Si(Li) detector] was going on.

The thin foil for the fluorescence measurements was mounted in a small vacuum chamber in order to reduce the signal of coherently and incoherently (in air) scattered primary x rays. The induced fluorescence was detected by a Si(Li) detector with an energy resolution of 210 eV full width at half maximum (FWHM) at 5.9 keV. In the data evaluation, (minor) corrections for the x-ray absorption in the sample were applied.

In the applied method it is necessary to determine the intensity of the L fluorescence of the investigated element at various primary photon energies with high accuracy. In order to overcome such problems as efficiency calibration of an ionization chamber and correction for dead-time losses of the x-ray detector we used a normalization to the K x-ray fluorescence of a light element. For this purpose, the previously described thin foil was sandwiched by another thin foil (Table I). By proper choice of a set of foils, e.g., Ta and Mn, the detector records the Ta L x rays simultaneously with the Mn K x rays (Fig. 4). The Mn K x radiation provides the normalization since in the measured range of primary photon energies its intensity depends smoothly on photon energy, i.e., $\sigma_K(E_\gamma) \propto E_\gamma^{-2.65}$, as predicted by theory[24] and confirmed by experiment.[25]

IV. L-SUBSHELL PHOTOIONIZATION CROSS SECTIONS

The applied method relies on well-known photoionization cross sections of the individual subshells. The theoretical treatment of photoionization is well developed[26] and comprehensive tabulations of calculated cross sections are available.[24] These relativistic Hartree-Slater (RHS) calculations have been performed with the following assumptions.

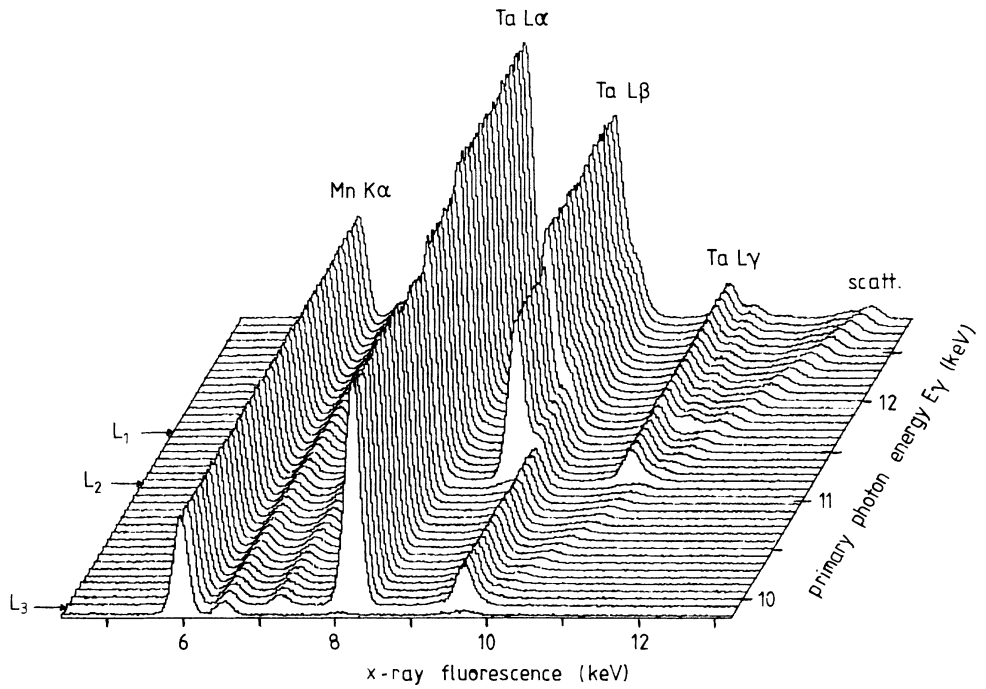

FIG. 4. X-ray fluorescence of a Mn-Ta sandwich sample excited by photons with different primary energies, as indicated on the right. All spectra are normalized to the same height of the Mn $K\alpha$ line. Clearly, the change of the Ta L spectrum at the Ta L edges can be seen. The small peak at the high-energy side of the fluorescence originates from coherently and incoherently scattered primary radiation.

(i) Electrons move in a Hartree-Slater potential which is assumed to be the same before and after the absorption of the photons.

(ii) Electrons are treated relativistically.

(iii) In the treatment of the radiation field all contributing multipoles and retardation effects are included.

Summing the ionization cross sections of all (sub)shells and the minor contribution of photon scattering, the photon absorption cross section is obtained. It can be directly measured in mass-attenuation studies. For the systems studied in the present work, the agreement between the calculations and experiment is 3–5% on an absolute scale.[25]

In spite of this good absolute agreement for the mass attenuation, we obtained inconsistent results when we tried to extract ionization cross sections of individual subshells from published attenuation cross sections[27] by extrapolation beyond the absorption edges. Therefore we decided to measure the mass attenuation in the regime of the L edges. Our experimental data exhibit characteristic dispersionlike deviations from the theoretical prediction (Fig. 5). The origin of these deviations has been identified as an electron-correlation effect which is neglected in the RHS calculations: The photon field acts on all atomic electrons; these react to the disturbance, thereby causing a dielectric screening or antiscreening of the external radiation field. Calculations in the time-dependent local-density approximation for the response of the electrons to the radiation field partly give a quantitative description of the effect on the total cross section. They also reveal that the effect is quite the same for the different subshells.[20] Therefore we decided to adopt the following expression as the best estimate for the actual ionization cross section σ^{act} of an individual L subshell:

$$\sigma_{L_i}^{\text{act}}(E_\gamma)=\sigma_{L_i}^{\text{fit}}(E_\gamma)[1+\Delta(E_\gamma)] , \tag{4}$$

where $\sigma_{L_i}^{\text{fit}}(E_\gamma)$ is an analytical fit to tabulated RHS calculations[24] and Δ is a small empirical correction (at most a few percent) which is independent of the individual subshell L_i and which is determined by the difference of calculated and experimental values of the total absorption cross section (sum over all contributing processes).

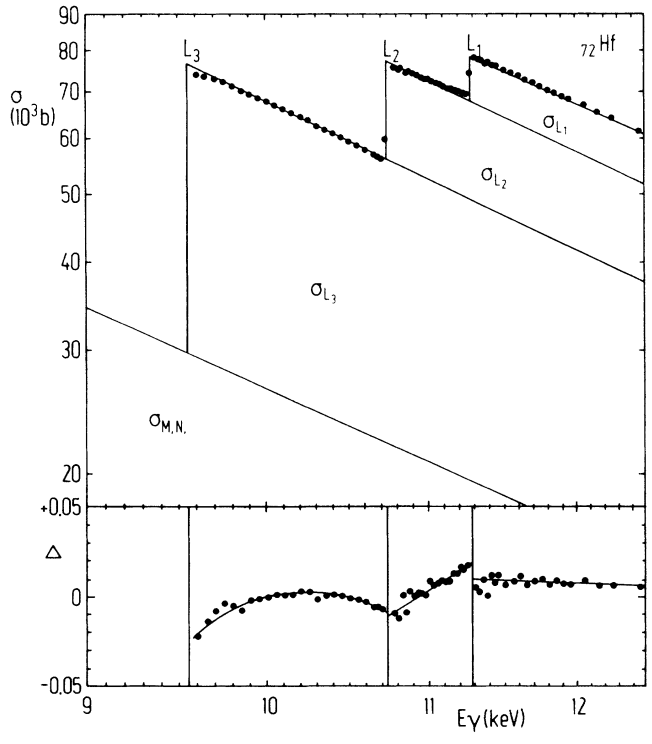

FIG. 5. Photoionization cross section of $_{72}$Hf vs photon energy E_γ in the regime of the L edges. Curves in the upper part are a theoretical prediction (Ref. 24). Dots are experimental data whose absolute values are normalized to theory. The lower part displays the deviation Δ between experiment and prediction as well as a fitted curve.

V. EXPERIMENTAL RESULTS

Comparison of the experimentally measured fluorescence at various photon energies with the ionization cross sections directly gives the Coster-Kronig yields and the ratios of fluorescence yields [Eqs. (1)-(3)]. The electron correlations have an effect on ionization cross sections with size in the percent realm; nevertheless, they may not be disregarded in the present case: they cause characteristic changes of subshell cross sections in the vicinity of the absorption edges; it is just the relative increase of the fluorescence intensity at an edge from which the Coster-Kronig yields are obtained. To get an estimate for the influence of the correlation effects on the obtained Coster-Kronig rates, we performed a data evaluation including [by the Δ term in Eq. (4)] or omitting ($\Delta \equiv 0$) the correlations (Fig. 6). Although the latter case is unrealistically worse, the two kinds of data evaluation give results with only minor deviations (Table II) and thus we are confident that the uncertainties of the correlations

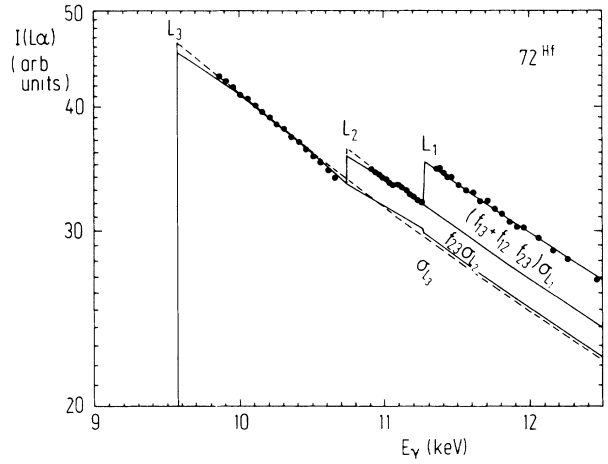

FIG. 6. Intensity of the Hf $L\alpha$ line vs primary photon energy E_γ. Dots are experimental data. Curves are fits according to Eq. (1) using subshell ionization cross sections [Eq. (4)] including (solid lines) and omitting (dashed lines) electron correlations.

TABLE II. Experimental values of the present work for the Coster-Kronig yields f_{23}, f_{12}, and f_{13} and the ratios of fluorescence yields ω_2/ω_3 and ω_1/ω_3. Values in parentheses have been obtained by omitting electron correlations in the data evaluation; they are regarded as incorrect and are only given for comparison purposes.

Z	f_{23}	f_{12}	$f_{13}+f_{12}f_{23}$	f_{13}	ω_2/ω_3	ω_1/ω_3
72	0.109±0.010	0.141±0.015	0.324±0.010	0.309±0.010	1.098±0.040	0.561±0.033
	(0.122±0.010)	(0.143±0.015)	(0.329±0.010)			
73	0.111±0.010	0.104±0.015	0.351±0.020	0.339±0.020	1.127±0.040	0.757±0.033
	(0.124±0.020)	(0.108±0.015)	(0.357±0.020)			
74	0.106±0.010	0.102±0.015	0.336±0.010	0.325±0.010	1.123±0.040	0.530±0.032
	(0.119±0.010)	(0.103±0.015)	(0.340±0.010)			
77	0.103±0.010	0.058±0.020	0.502±0.010	0.496±0.010	1.148±0.040	0.494±0.029
	(0.111±0.010)	(0.061±0.020)	(0.517±0.010)			
78	0.104±0.020	0.066±0.020	0.569±0.020	0.562±0.020	1.189±0.040	0.443±0.027
	(0.117±0.020)	(0.069±0.020)	(0.581±0.020)			
79	0.101±0.010	0.047±0.020	0.587±0.010	0.582±0.010	1.289±0.040	0.446±0.021
	(0.103±0.010)	(0.052±0.020)	(0.597±0.010)			
82	0.091±0.010	0.040±0.015	0.665±0.010	0.661±0.010	1.180±0.040	0.420±0.020
	(0.094±0.010)	(0.035±0.015)	(0.658±0.010)			

have almost negligible influence on the derived rates.

It is a challenge to compare our data (Fig. 7) to available experimental data obtained by different methods. The $K\alpha$-$L\alpha$ coincidence method is a powerful technique to measure accurately the parameters f_{23}, ω_2, and ω_3.[10] Recent measurements in Refs. 15–17 and 28, respectively, employing high-resolution x-ray detectors give results claiming impressive small uncertainties,

$$\begin{aligned} f_{23}(_{82}\mathrm{Pb}) &= 0.130\pm0.002 \\ &= 0.112\pm0.002 \\ &= 0.112\pm0.001 \\ &= 0.115\pm0.002 \ . \end{aligned} \tag{5a}$$

However, the first measurement[15] is strongly discrepant to the other measurements, indicating that systematic problems of the coincidence method are not under control. These problems are apparently not yet solved, since recent results, from Refs. 29 and 28, respectively, still deviate,

$$\begin{aligned} f_{23}(_{77}\mathrm{Ir}) &= 0.100\pm0.015 \ , \\ f_{23}(_{78}\mathrm{Pt}) &= 0.112\pm0.004 \ , \end{aligned} \tag{5b}$$

although we expect almost the same f_{23} for the two neighboring elements. Our values, i.e.,

$$\begin{aligned} f_{23}(_{78}\mathrm{Pt}) &= 0.104\pm0.020 \ , \\ f_{23}(_{82}\mathrm{Pb}) &= 0.091\pm0.010 \ , \end{aligned} \tag{5c}$$

lie systematically somewhat below the other mentioned experimental values and below the adopted values which are based on theory[12] (Fig. 7). It is not clear if the origin

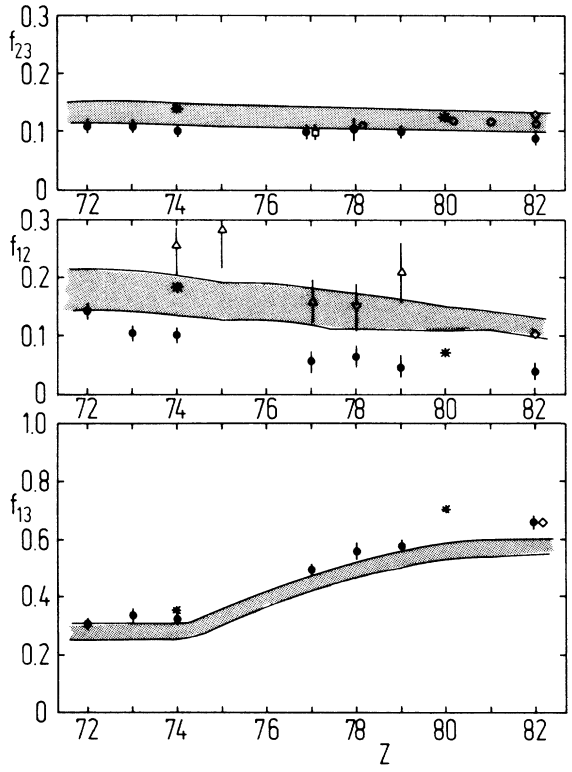

FIG. 7. Coster-Kronig factors f_{23}, f_{12}, and f_{13}. Experimental data: ●, present work; ○, Campbell and McGhee (Ref. 28); □, Rao (Ref. 29); ◇, Tan *et al.* (Ref. 15); △, Salgueiro *et al.* (Ref. 33); ▽, Marques *et al.* (Ref. 34). Theory: *, Chen *et al.* (Ref. 9). The dashed areas indicate the adopted values with estimated uncertainties (Ref. 12).

of the deviating results obtained by the coincidence and by the photoionization method stems from unrecognized instrumental problems or from the different processes of vacancy creation. f_{23} is dominantly determined by the L_2-L_3N transition (Fig. 1) which is susceptible to outer-shell spectator vacancies. The coincidence method relies first on the K-shell electron capture which produces negligible simultaneous outer-shell excitation[30] and, second, on the subsequent K-L_2 x-ray decay, which has about 10^{-2} probability for creating an N spectator.[31] In the photoionization method, the N-shell shake-off probability also amounts to 10^{-2}.[32] Thus the number of N-shell spectators is too small to account for the observed deviations.

In the L_1-vacancy decay, the f_{13} Coster-Kronig transition is dominant. The value of f_{13} increases by a factor of 2 (Fig. 7) while going from $Z=72$ to 82 due to the onset of the strong L_1-$L_3M_{4,5}$ Coster-Kronig channel (Fig. 1). Our data lie somewhat above the adopted values.[12] Since (for $Z \geq 76$) the procedure of the complication gives "f_1 values that are 10–15 % lower than the majority of the measured values,"[12] we are in good agreement with other experimental work.

Our f_{12} values are the most surprising result of all Coster-Kronig yields since they are substantially below the few available experimental data and also below the theory. Nevertheless, we have high confidence in our f_{12} values since these have been determined analogous to the other Coster-Kronig values and since our method of data taking is a direct one: while scanning the energy of the primary photons across the L_1 edge (Fig. 4), we observe only a tiny increase of the $L\gamma_1$ line (originating from the L_2 subshell), which is a direct indication of the smallness of f_{12}. All other experimental methods to determine f_{12} are indirect: e.g., Salgueiro *et al.*[33] excited the L fluorescence by electron impact and derived f_{12} from the intensity ratio of the $L\gamma_1$ satellite line to the $L\gamma_1$ parent line. However, the satellite line establishes itself only as a small asymmetry of the measured line, and thus the procedure of line analysis (which is not explained in their paper) may be easily susceptible to systematic errors. More recent work on f_{12} employed radioactive sources.[15,34] In this work the L_2 fluorescence is measured and its intensity is found to be larger than expected solely from the summed L_2 vacancy creation by direct excitation in the nuclear disintegration and by indirect excitation via the Auger decay of K vacancies. The excess intensity is assumed to originate from the f_{12} Coster-Kronig vacancy transfer. Experimentally it is obtained as the small difference of measured and expected (without Coster-Kronig contribution) intensity and thus its value is easily susceptible to errors in the assumed number of primary vacancies in the various shells created by the nuclear disintegration.

Our fluorescence-yield data are displayed in Fig. 8; only the ratios ω_2/ω_3 and ω_1/ω_3 are given, which are experimentally obtained without calibration of absolute detector efficiency, detection solid angle, etc. Our ω_2/ω_3 value for $Z=79$ and our ω_1/ω_3 value for $Z=73$ appear to be somewhat large as compared to the corresponding

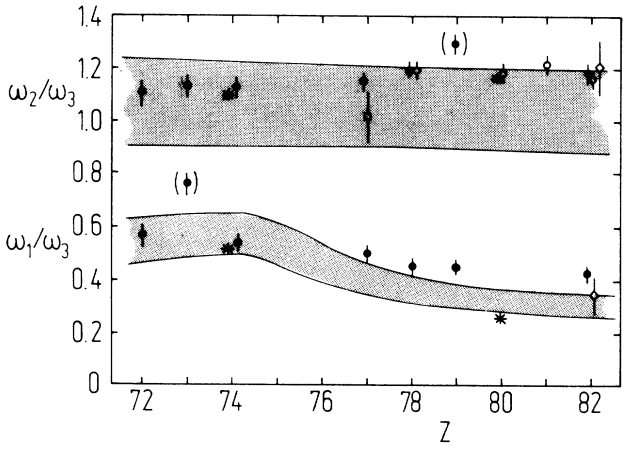

FIG. 8. Ratios of fluorescence yields ω_2/ω_3 and ω_1/ω_3. The meaning of the symbols is the same as in Fig. 7. The two values in parentheses are presumably outliers due to experimental problems.

values of neighboring elements. We attribute this to unidentified experimental problems. Our data for ω_2/ω_3 can be compared to other experimental work, in particular, that obtained by the $K\alpha$-$L\alpha$ coincidence method. They agree excellently with the data of Campbell and McGhee;[28] there are discrepancies to the data of Rao[29] similar to the discrepancies observed above for f_{23}. For the ratio ω_1/ω_3 other experimental data are scarce and almost all have been obtained by making specific assumptions. Therefore we refrain here from a comparison to other data.

VI. COMPARISON OF EXPERIMENTAL AND THEORETICAL ABSOLUTE TRANSITION RATES

Theory calculates absolute decay rates. A decisive comparison of experiment and theory should be performed on the basis of absolute rates since a comparison of yields, i.e., relative rates, might led to misleading results: For example, in the case when a particular decay channel is strongly dominant, its yield will always be close to unity, almost independent of the exact value of the absolute decay rate; in contrast, the yield of a weak channel depends then almost linearly on the rate of the strongly dominant channel, due to the normalization of the total yield to unity.

In order to convert our experimental data to absolute rates we proceed as follows. First, we make a choice for ω_3 and calculate ω_2 and ω_1. Second, we adopt calculated radiative decay rates for the three individual L subshells and calculate the nonradiative rates. In the choice of ω_3 one may adopt Krause's values which have an estimated uncertainty of 3–5 %.[12] Recent experimental values by Campbell and McGhee[28] are about 7% smaller than Krause's values and have an estimated uncertainty of 2%; they are available only for some of the investigated elements. We decided to adopt 0.96 times Krause's value as the best estimate of ω_3 for all investigated elements.

TABLE III. The experimental data of the present work (Table II) have been converted to the fluorescence yields ω_2 and ω_1 and Auger-yields a_3, a_2, and a_1 by adopting for the L_3-fluorescence yield the value given in the first column, i.e., 0.96 times the value of Krause (Ref. 12). The abbreviation "est. unc." denotes the estimated uncertainty.

Z	ω_3	ω_2	ω_1	a_3	a_2	a_1
72	0.222	0.243	0.125	0.778	0.648	0.425
73	0.233	0.262		0.767	0.627	
74	0.245	0.274	0.130	0.755	0.620	0.443
77	0.282	0.323	0.139	0.718	0.574	0.307
78	0.294	0.349	0.130	0.706	0.547	0.242
79	0.307		0.137	0.693		0.234
82	0.346	0.408	0.145	0.654	0.501	0.154
Est. unc.	±4%	±6%	±6%	±4%	±6%	±6%

Then it is trivial to calculate the fluorescence yields ω_2 and ω_1 from our measured ratios ω_2/ω_3 and ω_1/ω_3 (Table III). With values for the fluorescence yields, the Auger yields are easily deduced from the normalization of all yields to unity (Table III),

$$\begin{aligned} a_3 &= 1-\omega_3 , \\ a_2 &= 1-\omega_2-f_{23} , \\ a_1 &= 1-\omega_1-f_{12}-f_{13} . \end{aligned} \tag{6}$$

Since now all yields have been determined, one can proceed to convert the yields to absolute transition rates Γ. For the conversion, we adopt the radiative rates $\Gamma(\omega_i)$ for the individual subshells i as predicted by theory.[5]

The nonradiative rates $\Gamma(f_{ij})$ and $\Gamma(a_i)$ of a Coster-Kronig and an Auger transition, respectively, from a particular subshell can be expressed in terms of the corresponding radiative rate $\Gamma(\omega_i)$ and the various yields

$$\begin{aligned} \Gamma(f_{23}) &= \Gamma(\omega_2) f_{23}/\omega_2 , \\ \Gamma(f_{12}) &= \Gamma(\omega_1) f_{12}/\omega_1 , \\ \Gamma(f_{13}) &= \Gamma(\omega_1) f_{13}/\omega_1 , \\ \Gamma(a_3) &= \Gamma(\omega_3) a_3/\omega_3 , \\ \Gamma(a_2) &= \Gamma(\omega_2) a_2/\omega_2 , \\ \Gamma(a_1) &= \Gamma(\omega_1) a_1/\omega_1 . \end{aligned} \tag{7}$$

For the conversion of our experimental data to absolute transition rates we have chosen the calculated radiative rates $\Gamma(\omega_i)$, since they are expected to be the most reliable rates: The radiative decay is essentially a single-electron process and Hartree-Fock calculations yield reliable results; in particular, (i) calculated rates agree with measured $K\alpha$ linewidths[35] of the heavy elements in which the radiative component predominates and (ii) calculated cross sections of the similar photoionization process agree with experiment within at least a few percent.[25] We estimate a similar uncertainty, say ±4%, for the calculated radiative rates.

In a comparison of theoretical and experimental decay rates (Table IV, Fig. 9), we make the simplifying assumption that the L-decay yields are the same if the atom initially possess only one vacancy (direct vacancy production) or possess an additional spectator vacancy (vacancy production via a Coster-Kronig cascade). This assumption seems justified at the present level of experimental

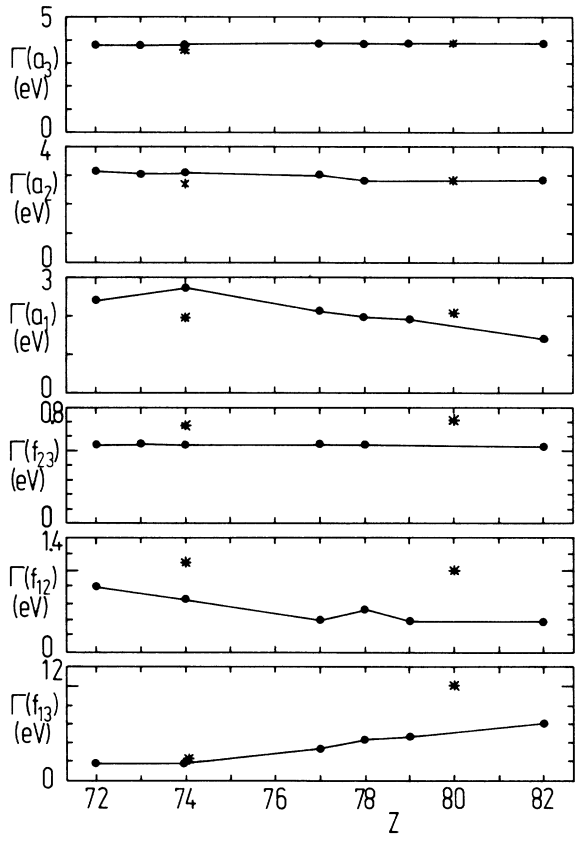

FIG. 9. Absolute decay rates of the various nonradiative L-subshell decay modes. Asterisks denote theoretical values (Ref. 9), points are experimental data of the present work, which have been connected by straight lines to guide the eye.

TABLE IV. The experimental values of the present work for the Auger yields a_3, a_2, and a_1 and the Coster-Kronig yields f_{23}, f_{12}, and f_{13} (Tables II and III) have been converted to absolute transition rates by using the absolute radiative transition rates from Scofield (Ref. 5) as given in the first three data columns.

Z	$\Gamma(\omega_3)$ (eV)	$\Gamma(\omega_2)$ (eV)	$\Gamma(\omega_1)$ (eV)	$\Gamma(a_3)$ (eV)	$\Gamma(a_2)$ (eV)	$\Gamma(a_1)$ (eV)	$\Gamma(f_{23})$ (eV)	$\Gamma(f_{12})$ (eV)	$\Gamma(f_{13})$ (eV)
72	1.087	1.214	0.701	3.809	3.236	2.395	0.544	0.794	1.739
73	1.163	1.303	0.752	3.828	3.120		0.552		
74	1.244	1.397	0.805	3.834	3.154	2.747	0.540	0.632	2.015
77	1.513	1.718	0.982	3.852	3.055	2.162	0.548	0.409	3.496
78	1.612	1.836	1.048	3.871	2.882	1.945	0.548	0.531	4.522
79	1.717	1.926	1.117	3.876		1.910		0.383	4.748
82	2.060	2.378	1.350	3.894	2.925	1.428	0.531	0.372	6.141
Estimated uncertainty	±5%	±5%	±5%	±8%	±10%	±10%	±12%	±20%	±8%

uncertainty. Comparison of theory and experiment (Table IV, Fig. 9) reveals reasonable agreement for the Auger rates $\Gamma(a_3)$, $\Gamma(a_2)$, and $\Gamma(a_1)$ and—to some extent—also for the Coster-Kronig rate $\Gamma(f_{23})$, but significant discrepancies are observed for $\Gamma(f_{12})$ (for all Z) and $\Gamma(f_{13})$ (for $Z=80$). It is well known that theory overestimates the Coster-Kronig rates in general[12] and $\Gamma(f_{13})$ for $Z=80$ in particular.[36] A detailed look at the various channels contributing to a Coster-Kronig rate (Fig. 1) indicates that in those cases in which the excess energy carried away by the emitted electron is larger than the energy differences between the L subshells (a few keV) the nonradiative rates are well predicted by theory, whereas in those cases in which the excess energy is smaller (particularly below 1 keV) the rates are strongly overestimated. Presumably, in the case of excess energy significantly smaller than the energy of the initial vacancy state the theoretical perturbation approach assuming frozen orbitals[6] is inadequate.

VII. CONCLUSIONS

The novel method of synchrotron photoionization has proved to be a powerful technique to measure decay yields of all L subshells accurately. It is a direct method relying only on accurate photoionization cross sections which can be obtained from mass-attenuation studies. It complements the $K\alpha$-$L\alpha$ coincidence method which gives smaller uncertainties but is applicable only for the L_2 and L_3 subshells and not for the L_1 subshell. The two methods provide agreeing values for the ratio of fluorescence yields ω_2/ω_3, whereas a minor deviation is observed for f_{23}. The origin of the deviation is not clear; it may be of experimental nature (unidentified experimental problem) or of physical nature (different way of primary vacancy creation).

Our comprehensive experimental data have been converted to absolute transition rates by adopting calculated radiative rates. Comparison with calculated nonradiative rates shows that the standard theory predicts nonradiative rates reasonably well in those cases in which the excess energy of a decay channel is comparable with the energy of the initial vacancy state, and that it severely overestimates the rates in cases in which the excess energy is significantly smaller.

Comprehensive measurements by the synchrotron-photoionization method are now required to produce a reliable set of decay yields for the L subshells of elements with medium and low atomic number Z. Discontinuities at certain Z, as well as a dependence on phase state (gaseous phase, condensed matter) have to be studied in detail. It remains a challenge to extend this work to the M subshells, where available information is scarce.

ACKNOWLEDGMENTS

Valuable discussions with Professor Dr. H. O. Lutz and the productive collaboration with Dr. G. Materlik and K. Finck are gratefully acknowledged. This work was supported by the Minister für Wissenschaft und Forschung des Landes Nordrhein-Westfalen.

[1]C. J. Powell, in *Proceedings of the Seventh International Vacuum Congress and the Third International Conference on Solid Surfaces,* edited by R. Dobrozemsky, F. Rüdenauer, F. P. Viehböck, and A. Breth (Dobrozemsky, Vienna, 1977), p. 2319.

[2]W. Jitschin, Nucl. Instrum. Methods B **4**, 292 (1984).

[3]M. P. Seah, Vacuum **36**, 399 (1986).

[4]W. Jitschin and U. Werner, J. Vac. Sci. Technol. A **5**, 1203 (1987).

[5]J. H. Scofield, At. Data Nucl. Data Tables **14**, 121 (1974).

[6]M. H. Chen, B. Crasemann, and H. Mark, At. Data Nucl. Data Tables **24**, 13 (1979).

[7]M. H. Chen, B. Crasemann, K.-H. Huang, M. Aoyagi, and H. Mark, At. Data Nucl. Data Tables **19**, 97 (1977).

[8]Kh. R. Karim and B. Crasemann, Phys. Rev. A **31**, 709 (1985).

[9]M. H. Chen, B. Crasemann, and H. Mark, Phys. Rev. A **24**,

177 (1981).
[10]W. Bambynek, B. Crasemann, R. W. Fink, H.-U. Freund, H. Mark, C. D. Swift, R. E. Price, and P. V. Rao, Rev. Mod. Phys. **44**, 716 (1972).
[11]P. V. Rao, in *Atomic Inner-Shell Processes,* edited by B. Crasemann (Academic, New York, 1975), p. 1.
[12]M. O. Krause, J. Phys. Chem. Ref. Data **8**, 307 (1979).
[13]A. Langenberg and J. v. Eck, J. Phys. B **12**, 1331 (1979).
[14]H. Paul and J. Muhr, Phys. Rep. **135**, 47 (1986).
[15]M. Tan, R. A. Braga, R. W. Fink, and P. V. Rao, Phys. Scr. **25**, 536 (1982).
[16]J. L. Campbell, P. L. McGhee, R. R. Gingerich, R. W. Ollerhead, and J. A. Maxwell, Phys. Rev. A **30**, 161 (1984).
[17]A. L. Catz, Phys. Rev. A **36**, 3155 (1987).
[18]W. Jitschin, G. Materlik, U. Werner, and P. Funke, J. Phys. B **18**, 1139 (1985).
[19]W. Jitschin, U. Werner, K. Finck, and H. O. Lutz, in *High-Energy Ion-Atom Collision II,* edited by D. Berényi and G. Hock (North-Holland, Amsterdam, 1985), p. 79.
[20]W. Jitschin, U. Werner, G. Materlik, and G. D. Doolen, Phys. Rev. A **35**, 5038 (1987).
[21]U. Werner and W. Jitschin, J. Phys. (Paris) Colloq. **48**, C9–559 (1987).
[22]G. Materlik and V. O. Kostroun, Rev. Sci. Instrum. **51**, 86 (1980).
[23]J. A. Bearden and A. F. Burr, Rev. Mod. Phys. **39**, 125 (1967).
[24]J. H. Scofield, Lawrence Livermore Radiation Laboratory Report No. UCRL-51326, 1973 (unpublished).
[25]J. H. Hubbell and Wm. J. Veigele, Nat. Bur. Stand. (U.S.) Technical Note No. 901 (U.S. GPO, Washington, D.C., 1976).
[26]J. W. Cooper, in *Atomic Inner-Shell Processes,* edited by B. Crasemann (Academic, New York, 1975), p. 159.
[27]Wm. J. Veigele, At. Data Tables **5**, 51 (1973).
[28]J. L. Campbell and P. L. McGhee, J. Phys. (Paris) Colloq. **48**, C9-597 (1987); P. L. McGhee and J. L. Campbell, J. Phys. B **21**, 2295 (1988).
[29]P. V. Rao, Book of Abstracts Fourteenth International Conference on X-Ray and Inner-Shell Processes X87, Paris, 1987, edited by P. Lagarde, F. J. Wuilleumier, and J. P. Briand (unpublished), p. B-b 13.
[30]P. G. Hansen, B. Jonson, G. L. Borchert, and O. W. B. Schult, in *Atomic Inner-Shell Physics* edited by B. Craseman (Plenum, New York, 1985), p. 237.
[31]G. L. Borchert, P. G. Hansen, B. Jonson, I. Lindgren, H. L. Ravn, O. W. B. Schult, and P. Tidemand-Petersson, Phys. Lett. **65A**, 297 (1978).
[32]N. M. Mirakhmedov and E. S. Parilis, in *X84 X-Ray and Inner-Shell Processes in Atoms, Molecules and Solids,* edited by A. Meisel and J. Finster (Karl-Marx-Universität, Leipzig, 1984), p. 177.
[33]L. Salgueiro, M. T. Ramos, M. L. Escrivão, M. C. Martins, and J. G. Ferreira, J. Phys. B **7**, 342 (1974).
[34]M. I. Marques, M. C. Martins, and J. G. Ferreira, Phys. Scr. **32**, 107 (1985).
[35]S. I. Salem and P. L. Lee, At. Data Nucl. Data Tables **18**, 233 (1976).
[36]O. Keski-Rahkonen, G. Materlik, B. Sonntag, and J. Tulkki, J. Phys. B **17**, L121 (1984).

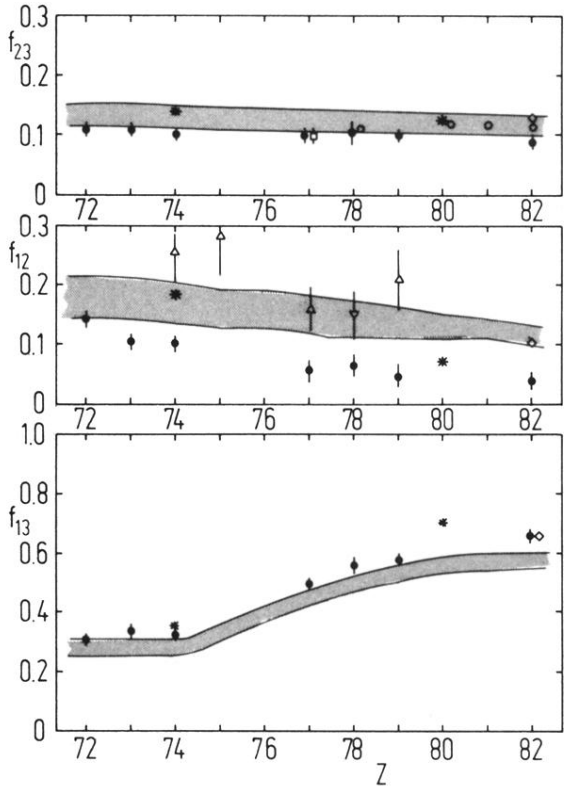

FIG. 7. Coster-Kronig factors f_{23}, f_{12}, and f_{13}. Experimental data: ●, present work; ○, Campbell and McGhee (Ref. 28); □, Rao (Ref. 29); ◇, Tan *et al.* (Ref. 15); △, Salgueiro *et al.* (Ref. 33); ▽, Marques *et al.* (Ref. 34). Theory: ∗, Chen *et al.* (Ref. 9). The dashed areas indicate the adopted values with estimated uncertainties (Ref. 12).

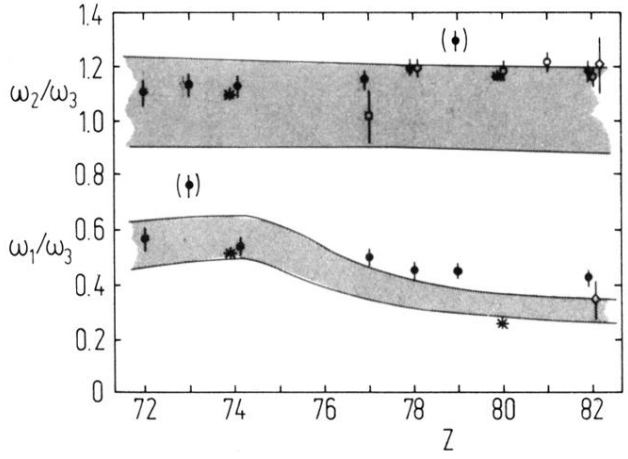

FIG. 8. Ratios of fluorescence yields ω_2/ω_3 and ω_1/ω_3. The meaning of the symbols is the same as in Fig. 7. The two values in parentheses are presumably outliers due to experimental problems.